







Article

The Leaky-Wave Perspective for Array-Fed Fabry–Perot Cavity and Bull’s-Eye Antennas

Mikhail Madji ¹, Edoardo Negri ¹, Walter Fuscaldo ², Davide Comite ¹, Alessandro Galli ^{1,*}
and Paolo Burghignoli ¹

¹ Department of Information Engineering, Electronics and Telecommunications, Sapienza University of Rome, 00184 Rome, Italy; mikhail.madji@uniroma1.it (M.M.); edoardo.negri@uniroma1.it (E.N.); davide.comite@uniroma1.it (D.C.); paolo.burghignoli@uniroma1.it (P.B.)

² Istituto per la Microelettronica e Microsistemi, Consiglio Nazionale delle Ricerche, 00133 Rome, Italy; walter.fuscaldo@cnr.it

* Correspondence: alessandro.galli@uniroma1.it

Abstract: Two-dimensional leaky-wave antennas (LWAs) are a class of planar, traveling-wave radiators with attractive features of a low profile, ease of feeding, frequency reconfigurability of the radiation pattern, and polarization agility. Their use in conjunction with array feeders has been the subject of various investigations in recent decades, thanks to the additional degrees of freedom provided by the presence of multiple independent sources. Here, we provide a review of some of the most recent and promising array-fed two-dimensional (2-D) LWAs, selecting a couple of the most significant structures in application, namely Fabry–Perot cavity antennas and *bull’s-eye* antennas, and discussing some of their recently proposed advanced features.

Keywords: leaky-wave antennas; planar antennas; phased arrays; Fabry–Perot cavity antennas; *bull’s eye* antenna; orbital angular momentum; polarization reconfiguration; pattern reconfigurability; near-field focusing



Citation: Madji, M.; Negri, E.; Fuscaldo, W.; Comite, D.; Galli, A.; Burghignoli, P. The Leaky-Wave Perspective for Array-Fed Fabry–Perot Cavity and Bull’s-Eye Antennas. *Appl. Sci.* **2024**, *14*, 6775. <https://doi.org/10.3390/app14156775>

Academic Editors: Changfei Zhou and Min Li

Received: 20 June 2024

Revised: 28 July 2024

Accepted: 29 July 2024

Published: 2 August 2024



Copyright: © 2024 by the authors. Licensee MDPI, Basel, Switzerland. This article is an open access article distributed under the terms and conditions of the Creative Commons Attribution (CC BY) license (<https://creativecommons.org/licenses/by/4.0/>).

1. Introduction

Two-dimensional (2-D) leaky-wave antennas (LWAs) belong to the class of traveling-wave antennas. Based on planar geometries, either metallic or metal-dielectric, their working principle depends on the excitation on the antenna aperture of *cylindrical leaky waves*, excited by a simple nondirective source and propagating with a complex leaky radial wavenumber $k_\rho = \beta - j\alpha$ (with respect to the cylindrical coordinates reported in Figure 1), with β and α being the radial leaky phase and attenuation constants, respectively [1,2].

Leaky waves in uniform open waveguides made using ordinary materials are *improper* solutions of the relevant dispersion equations, i.e., they do not satisfy the Sommerfeld radiation condition at infinity [3–5], while they may be either proper or improper in periodic open waveguides [6], depending on the operating frequency. In any case, their physical validity is restricted to certain angular ranges within which they are exponentially damped and hence negligible at infinity; nevertheless, if they are effectively excited in frequency ranges where they are both fast ($|\beta| < k_0$) and characterized by an attenuation constant that is small with respect to the free-space wavenumber k_0 ($\alpha \ll k_0$), they may dominate the antenna aperture field: leaky waves can therefore provide an asymptotic representation of the relevant waveguide continuous spectrum and thus, via Fourier transformation, of the antenna radiation pattern [7,8].

The condition $\alpha \ll k_0$, crucial for the leaky wave to dominate the aperture field, implies that the complex wave provides a large aperture illumination, in terms of the free-space wavelength λ_0 . An immediate consequence is that, considering the properties of the Fourier transform, the radiation pattern is characterized by high directivity in elevation.

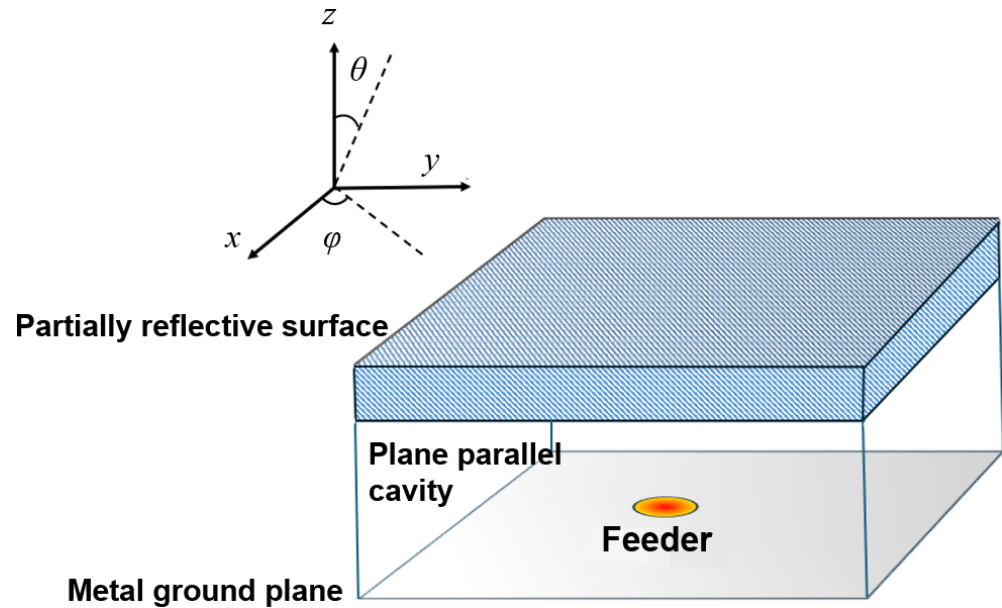


Figure 1. Pictorial representation of a Fabry–Perot Cavity antenna (FPCA), with the relevant reference system.

A cylindrical leaky wave with $\beta > \alpha$ radiates a conical scanned beam with pointing angle $\theta_0 > 0$, whereas, when $\beta \leq \alpha$, a broadside beam ($\theta_0 = 0$) is produced [7]. Two important formulas for the pointing angle θ_0 and the -3 dB elevation beamwidth $\Delta\theta$, valid for the case of a scanned beam, are (1)

$$\theta_0 \simeq \arcsin \hat{\beta} \quad \Delta\theta \simeq 2\hat{\alpha} \sec \theta_0 \quad (1)$$

where the hat $\hat{\cdot}$ indicates the normalization of radial phase and attenuation constants β and α , respectively, by the free-space wavenumber k_0 (additional general pattern-related formulas may be found in [7,9,10], for a great variety of cases encountered in applications). The normalized radial wavenumber \hat{k}_ρ typically shows a frequency-dispersive behavior. Therefore, as a consequence of (1), to perform an elevation scan (and also potentially change the elevation beamwidth), it is sufficient to vary the operating frequency [11–13].

The aim of this work is to introduce 2-D LWAs with multiple feeders, i.e., array-fed 2-D LWAs. In such designs, the attractive features of LWAs in terms of elevation directivity, pattern reconfigurability, and feed simplicity are combined with additional degrees of freedom. In particular, there is the possibility to independently control multiple sources in amplitude and phase, thus shaping the associated array factor. Although various other 2-D LWAs exist (such as holographic [14,15] and modulated surface antennas [16–19]), here we specifically address two categories, namely Fabry–Perot cavity antennas (FPCAs) and *bull’s-eye* antennas (BEAs). In Section 2, we present array-fed implementations of the former class, whereas the latter configuration with multiple feeders is discussed in Section 3. Finally, conclusions are drawn in Section 4.

2. Fabry–Perot Cavity Antennas

Fabry–Perot cavity antennas represent a class of resonant radiating systems. The first evidence of such structures was found in the last quarter of the 19th century, when Fabry–Perot interferometers were developed at the time presenting exceptional, unprecedented spectroscopic resolving powers [20]. The idea behind FPCAs, first proposed in [21], stemmed from the intuition that such a high optical wavelength resolution could be turned into angular resolution and hence high elevation directivity in the microwave range.

A plane-parallel cavity represents the core of the structure, enclosed by a metal ground plane and a partially reflective sheet (PRS), either uniform (e.g., a high-permittivity super-

strate) or quasi-uniform (e.g., a periodic metal screen with spatial periods that are small with respect to the free-space wavelength) [22,23] (see Figure 1).

Even if the first attempt to theoretically obtain a collimated beam at broadside was based on geometrical optics [21,24,25], the leaky-wave method has proven to be more physically insightful and effective in the design procedure [26,27]. In this light, antenna feeders have the role of efficiently exciting cylindrical leaky waves; hence, they are typically simple, nondirective radiating elements such as dipoles, slots, or patch antennas. The source choice, however, directly affects the azimuthal dependence, as well as the polarization of the relevant excited field [7].

2.1. Fabry–Perot Cavities and Far-Field Twisted Beams

Recently, FPCAs have been employed in a number of cases to launch waves carrying orbital angular momentum (OAM) [28]. While polarization control is a widespread topic, OAM engineering has recently gained interest due to potential applications to telecommunications, radar, imaging, and sensing. Indeed, electromagnetic waves carrying different OAM states are orthogonal; thus, the bandwidth of a channel theoretically increases linearly with the number of OAM states [29,30].

OAM waves have been introduced in [31] for optical frequencies, rapidly finding interest in other bands, from radio frequencies up to X- and gamma-rays. Field twists are due to the phase distribution depending on the azimuth ϕ coordinate with the form $\exp(j\ell\phi)$, where ℓ is known as *topological charge*; its sign determines the handedness of the vortex and its absolute value the relevant number of twists in a period.

The interest in OAM waves mainly depends on the fact that, unlike circular polarization that is only able to provide right-handed or left-handed rotation, a potentially unlimited number of waves with different values of ℓ can be generated.

In a real-world scenario, OAM applications have limitations, mainly due to the phenomena of strong attenuation and fading [32,33]. One distinct issue consists in finding a suitable method of successful OAM excitation. It has been demonstrated that the most versatile method consists in circular arrays, which can be properly phased to obtain a radiated field transporting a given momentum. By switching from one inter-element phase difference value to another, the order of the momentum is varied. An issue for the latter scheme in the free-space configuration is the unavoidable dependence between the pointing angle and ℓ , as can be inferred from the expression of the radiation pattern below (2):

$$P^{\text{FS}}(\theta) = -2\pi j^\ell P_0 \sin \theta J_\ell(k_0 a \sin \theta) \tag{2}$$

where P_0 is the complex amplitude coefficient impressed to feeders, a is the radius of the array, and J_ℓ represents the first-kind Bessel function of ℓ -th order. When ℓ varies, the maximum of the pattern moves to different angles, for fixed values of array radius a and free-space propagation constant k_0 . This issue has been overcome by considering concentric circular arrays, one for each OAM order [34], increasing the overall number of feeders and the total complexity of the system. An alternative solution in order to reduce the number of sources was addressed in [28], where the effect of source embedding in Fabry–Perot cavities was considered. In a resonant environment, a simple planar circular array of coaxial feeders, approximated by vertical electrical dipoles (VEDs), is inserted through the ground plane of the cavity (see Figure 2). This choice is largely motivated by the fact that, according to (1), the main-beam features are mainly set by the radial wavenumber k_ρ of the operating leaky mode (3):

$$P^{\text{FP}}(\theta) = \frac{2 \cos \theta \csc k_{z\varepsilon} h P^{\text{FS}}(\theta) e^{jk_0 h \cos \theta}}{j\hat{k}_{z\varepsilon}(1 + \cos \theta \bar{Y}_{\text{PRS}}) + \varepsilon_r \cos \theta \cot k_{z\varepsilon} h} \tag{3}$$

in which $k_{z\varepsilon}$ corresponds to the complex transverse propagation constant [1], $\hat{k}_{z\varepsilon} = k_{z\varepsilon}/k_0$ is the relevant quantity normalized by the free-space wavenumber, $\bar{Y}_{\text{PRS}} = Y_{\text{PRS}}\eta_0$ is the

normalized sheet admittance of the PRS, η_0 is the free-space impedance, ϵ_r the value of dielectric constant of the material filling the cavity, and h the relevant height.

Observing the numerator in (3), the P^{FS} term is still present, but the nulls of the denominator, which appear due to the resonant nature of the cavity, mitigate the shifting effect due to OAM order selection, at least for low values of ℓ . Equivalently, such a condition can be explained by the dominance over the entire field of a singular spectral leaky contribution on the antenna aperture. Conversely, from the expression in (3), one may observe that a radiation null is always located at broadside [7,35]. Assigning to the VEDs a proper phasing scheme, it is possible to obtain a radiated field of a desired orbital angular order, selected from among $0, \pm 1, \pm 2, \pm 3$, without affecting the beam angle.

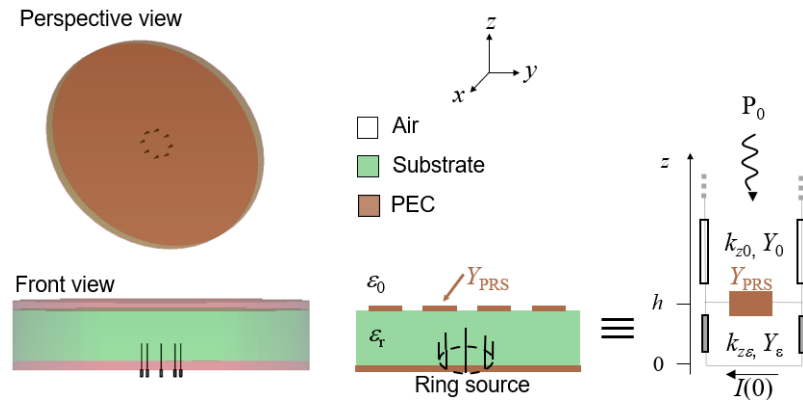


Figure 2. Model, perspective view, and transmission-line model of a circular array-fed Fabry-Perot cavity. Reproduced from [28].

It is worthwhile stressing that the latter result was obtained by reducing the TEM mode to a slow-wave regime filling the cavity with a low dielectric-constant material, and exciting the TM_1 mode in a fast-wave regime, with the relevant radial attenuation constant small enough to make the field dominant over the aperture, as shown in the dispersion diagram in Figure 3.

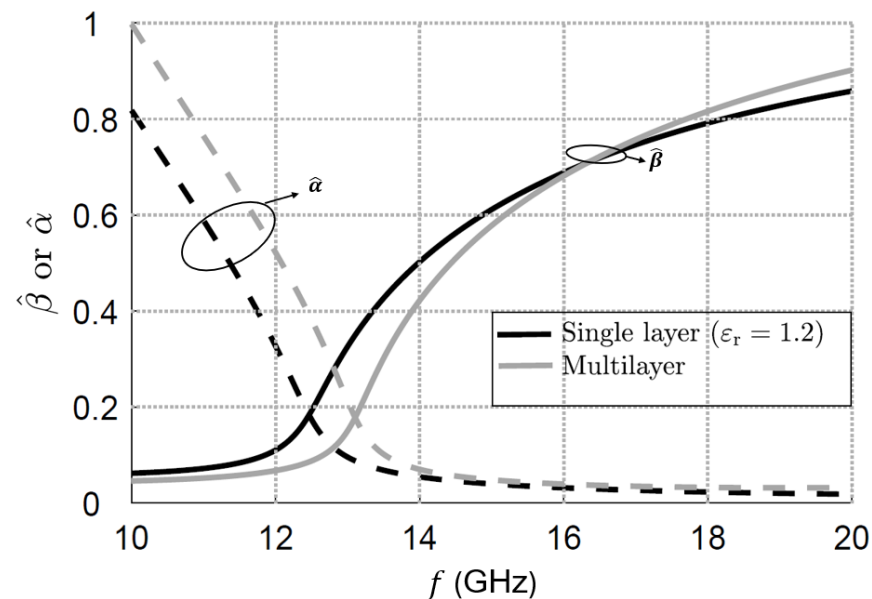


Figure 3. Dispersion diagram for the dominant TM_1 leaky mode supported by an FPCA. Two different curves for both phase and attenuation constants (represented by solid and dashed lines, respectively) correspond to two different low permittivity dielectrics, obtained respectively with a single layer and through a multilayer, reproduced from [28].

It is demonstrated that, referring to parameters chosen as in [28], a single dominant leaky solution is obtained around 18 GHz, whose relevant far-field pattern in the elevation plane is weakly affected by the chosen OAM order imposed by phasing, as shown in Figure 4.

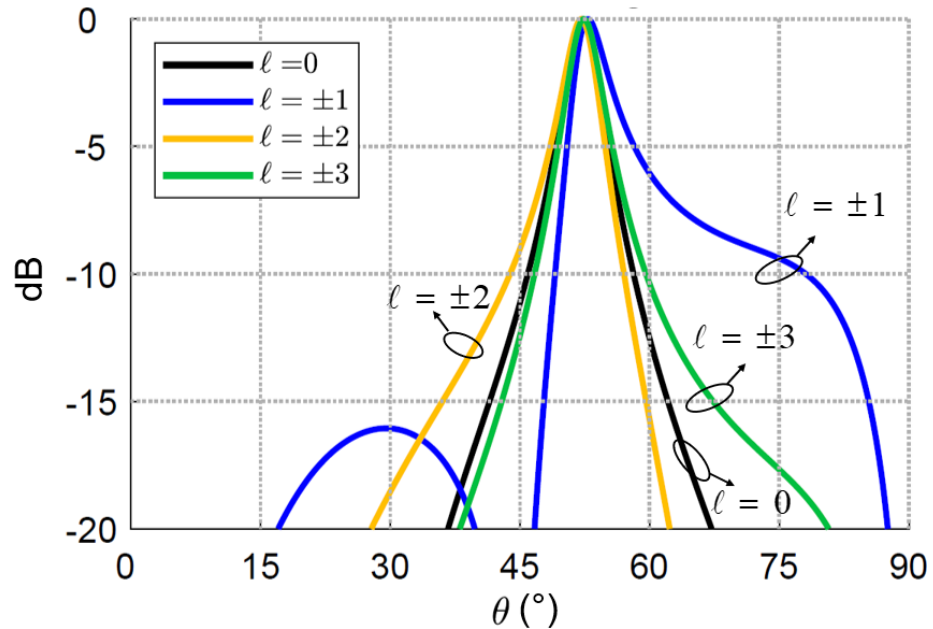


Figure 4. Normalized radiation pattern for the ideally infinite FPCA extension, at a frequency of 18 GHz, for an elevation angle of 52° , with the filling low-permittivity dielectric obtained with a single layer; further details and effects due to FPCA truncation are available in [28].

In Figure 5, the magnitudes of the scattering parameters are reported, demonstrating values lower than the -18 dB threshold, hence confirming an excellent excitation performance.

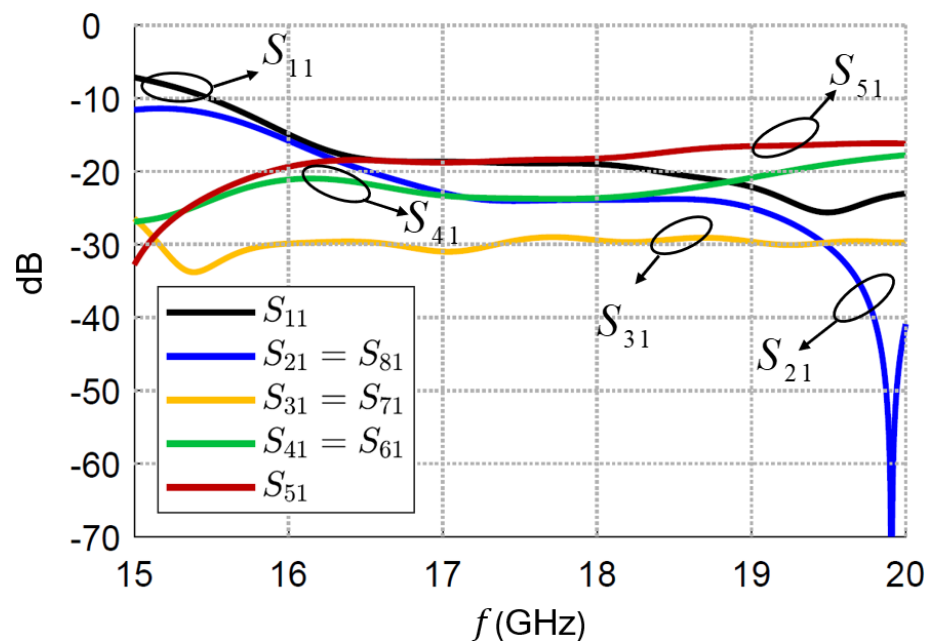


Figure 5. Reflection and transmission coefficients of the optimized FPCA feeding network. Due to the circular symmetry of the feeding array, a limited number of scattering parameters have been simulated and reported in [28].

2.2. Fabry–Perot Cavities for Far-Field Polarization Reconfiguration

Fabry–Perot cavity antennas find application in polarization reconfigurability and beam scanning. The demand for circular polarization is rapidly growing in the civil, medical, and military sectors, due to a number of advantages, such as the absence of orientation matching, resilience to multipath fading, and possibility to overcome obstacles on the propagation path [36]. Linear to circular conversion is a solution that may avoid complex geometries, to produce conditions of phase quadrature and magnitude equality on both horizontal and vertical field components. Once again, the 2-D LWAs and low-complexity standards required by relevant feeders may effectively simplify the design.

In [37], by independently exciting the fundamental TE–TM leaky mode pair, a simple polarization-reconfigurable elevation scan is obtained. The relevant feeding network consists of a coaxial cable inserted through the ground plane to obtain a VED-like source, whereas, by etching in the ground plane radial slits in a circular configuration, a source equivalent to a vertical magnetic dipole (VMD) is obtained (refer to [37] for an exhaustive geometrical description and parameters). Cavity optimization [38] gives a large frequency span (approximately from 12 to 19 GHz in the case considered in [37]), in which only a couple of TE and TM leaky modes with zeroth azimuthal order are independently excited by relevant sources.

In a homogenized regime where the PRS has a simple scalar description [39,40], a dispersion analysis may readily be carried out via the transverse resonance technique [1] to obtain and verify the equalization between TE and TM wavenumbers k_{ρ}^{TE} and k_{ρ}^{TM} . While attenuation-constant equalization is obtained through PRS design, the phase constants of the two modes are equalized by acting on the effective dielectric constant of the cavity: a wire medium (WM) layer can be inserted in a second low-permittivity dielectric, thus slowing down the phase velocity of the quasi-TEM mode. A sketch of the structure's geometry can be found in [37].

A single frequency optimization provided at 16 GHz [37] produces a noticeable broadband beam stability, in a range between 12 and 19 GHz (see Figure 6). Complex amplitudes for both VEDs and VMDs are chosen to obtain equal peak amplitudes and similar phase constants. Further, by simply imposing adequate complex amplitudes on feeders, it is shown that a swift polarization conversion is possible: a frequency-driven right-hand circularly polarized (RHCP) beam scan from an elevation angle of 30° to 70° was performed, with a low level of cross-polarized circular component, i.e., left-hand circular polarization (LHCP) component (see Figure 7).

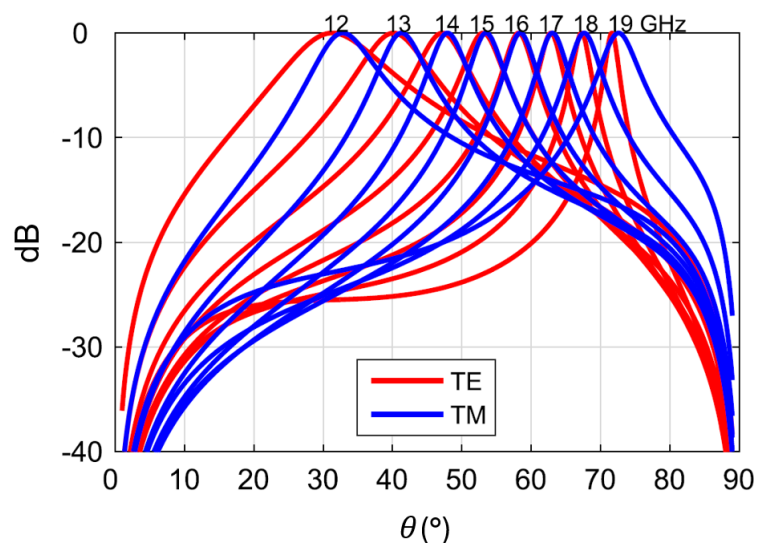


Figure 6. Frequency sweep and related beam scanning for produced TE and TM modes, over a frequency span between 12 and 19 GHz. Only a slight deviation from the equalization condition was observed around 12 and 19 GHz. Reproduced from [37].

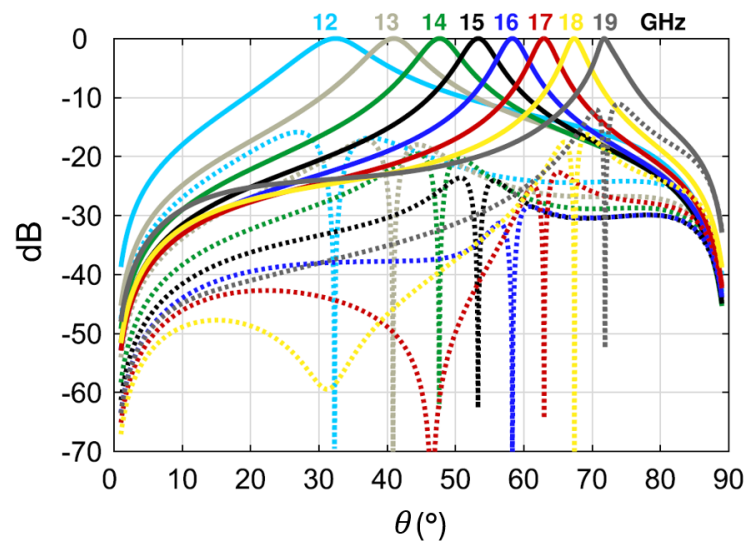


Figure 7. RHCP (solid lines) component frequency-scanning process in the elevation plane. As expected, the cross-polarized component (dotted lines) is negligible in a wide range of frequencies. Reproduced from [37].

The overall system, while not being able to scan too close to broadside due to constraints on far-field patterns generated by azimuthally invariant sources, demonstrates a versatile behavior in performing angular scan, both with linear and circular polarization.

2.3. Fabry–Perot Cavities for Beam Scanning in Elevation and Azimuth

Frequency scanning in elevation is a property of LWAs of considerable interest, albeit a full-beam control requires losing azimuth symmetry, and in turn the conical radiation pattern typical of FPCAs. Recently, a novel solution was proposed embedding a dipole array into the cavity, which allows us to vary the azimuth angle at which the radiation maximum is observed.

Limitations of free-space arrays are well-known, often requiring a very large number of elements. To avoid radiation through unwanted grating lobes, the spacing between adjacent elements should be smaller than half a free-space wavelength [41]. Meeting the above limitation may prove challenging, especially when the operating frequency is raised up to tens of GHz and beyond. The elevation selectivity of radiated leaky-wave beams allows us to significantly relax such a limit, given that an elevation-directive element pattern washes away lobes in the array factor. This latter aspect was proposed in [42] to find a profitable solution in array thinning to enlarge inter-element distance and reduce cross-talk phenomena. A grid of simple planar antennas were designed considering multi-layer dielectric structures, which in turn recreated a resonant environment and provided leaky-wave launching effect. Even without considering elements with high-gain features, the narrow-beam radiation element pattern of a single source relaxes requirements for the element spacing, mitigating the parasite coupling effects. The latter possibility was further developed in [43], when a dual-polarized antenna, constituted by two interleaved $N = 2 \times 2$ arrays, was employed, obtaining a high-gain radiation pattern in the far field. The seminal works in [42,43] constituted the starting point for the substantial part of the literature interested in compact high-gain antennas with reduced components cost and low fabrication complexity [44,45]. Further, novel features for FPCA-embedded sources have been studied, proposing different designs characterized by the common leaky nature of the relevant radiated fields.

The electronic reconfiguration of the radiation pattern, in particular of the beam angle in elevation, represents a critically interesting technology for a large number of applications, from satellite communications to radar, to mention but a few. This was studied in [46], once again considering an FPCA-embedded source array, composed of simple nondirectional VEDs in the form of coaxial probes, as illustrated in Figure 8.

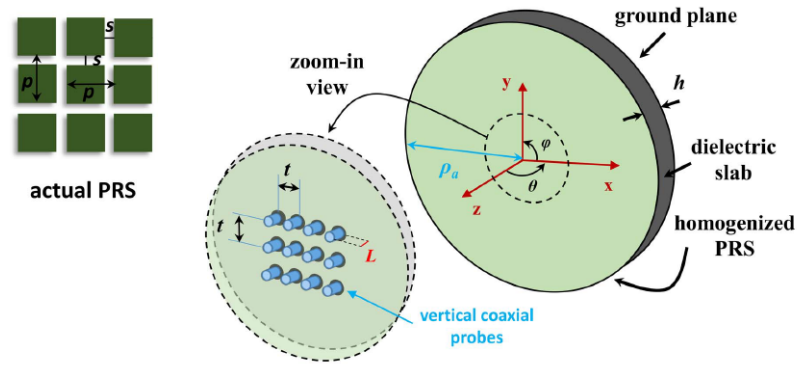


Figure 8. FPCA 3-D model and a planar feeding grid realized with coaxial cables. A schematic of the employed PRS is also reported. Reproduced from [46].

A PRS is designed by periodically patterning metallic square patches over a low-permittivity dielectric slab and making the quasi-TEM mode a slow wave, hence preventing it from radiating. The relevant inter-patch spacing is observed to weakly influence the phase constant of the excited TM_1 leaky-mode, while the attenuation constant shows a stronger dependence, as seen in Figure 9.

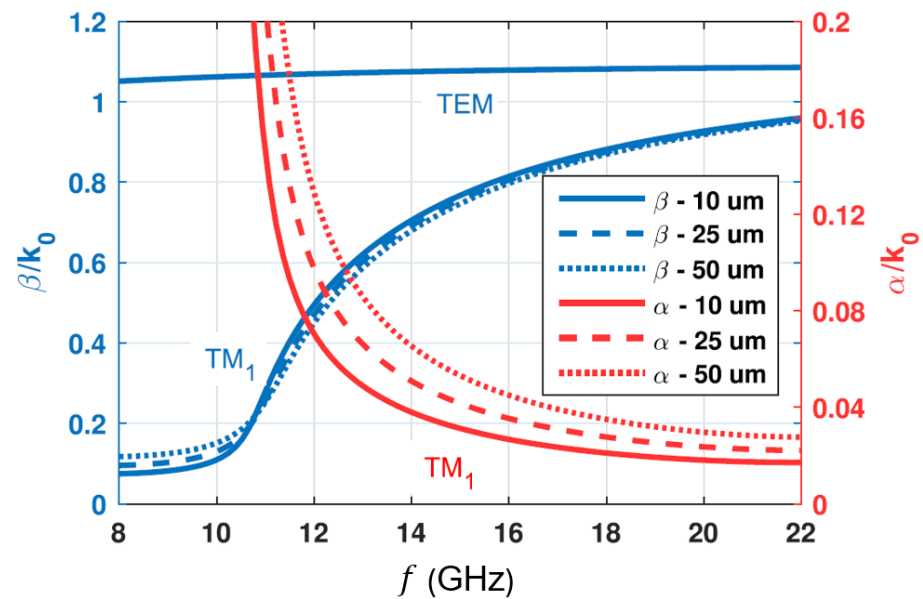


Figure 9. Dispersion of radial phase (blue lines) and attenuation constants (red lines) for multiple values of distance s between metallic patches composing the PRS. Higher values of s induce higher attenuation, while weakly affecting the phase constant. Reproduced from [46].

An optimal value of inter-patch spacing is found, since placing patches too close together results in a lower attenuation constant, which provides more selective beams in elevation plane but requires wider planar antenna extension to radiate up to 90% of available power and avoid edge diffraction. Additionally, for a single coaxial cable generating the relevant element pattern, an angular frequency-driven scan should be evaluated in the frequency range that ensures a satisfactory excitation of the cavity. Indeed, the overall frequency range, with a single leaky mode dominating the aperture, should be assessed to hold the magnitude of the input reflection coefficient, Γ_{in} , under the threshold of -10 dB. Considering limitations due the magnitude of the input reflection coefficient, an overall elevation scan was obtained from 45° to 60° [46]. Full-wave results obtained through reciprocity theorem were verified to be in good agreement with analytical leaky-wave patterns. Further comparison with the truncated version of the cylindrical wavefront model

was carried out taking into account the finite dimension of the cavity and relevant effects on the pattern [46], as shown in Figure 10.

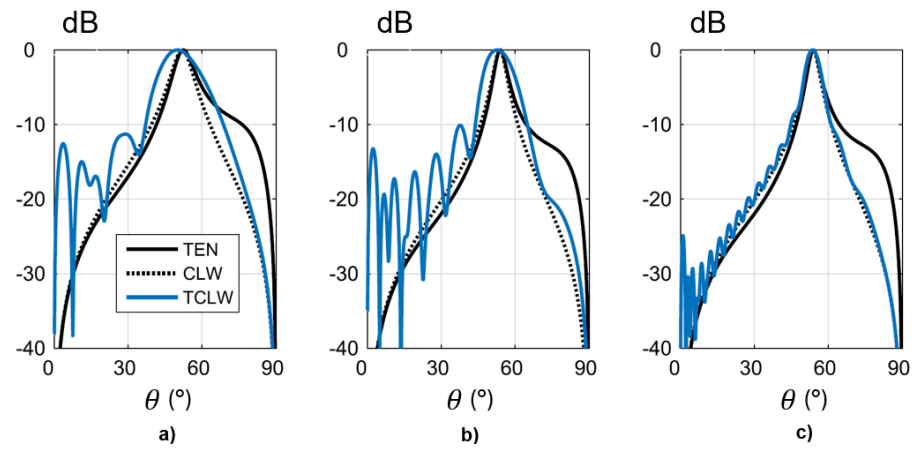


Figure 10. Cylindrical leaky-wave model, truncated cylindrical leaky-wave model, and reciprocity-obtained elevation pattern (TEN) at 16 GHz. (a) $s = 50 \mu\text{m}$, (b) $s = 10 \mu\text{m}$, (c) as in (b) but radiating 99% input power. Reproduced from [46].

Once element-pattern radiation capabilities have been assessed and validated by different approaches, multiple feeders are considered to extend the beam-scanning effect in the azimuthal dimension. A highly reduced number of $N \times N = 9$ VEDs is considered in a planar square grating, breaking the azimuthal invariance of the conically shaped element pattern with the multiplication by the scalar array factor, (4):

$$AP(\theta, \phi) = EP(\theta, \phi)AF(\theta, \phi) \tag{4}$$

where $AP(\theta, \phi)$ corresponds to the array pattern, $EP(\theta, \phi)$ to the element pattern, and $AF(\theta, \phi)$ to the scalar array factor. An expression for uniform arrays may be found in [41] for different planar geometries. Beam-shaping effects are shown, for multiple frequencies, in Figure 11, through directivity patterns.

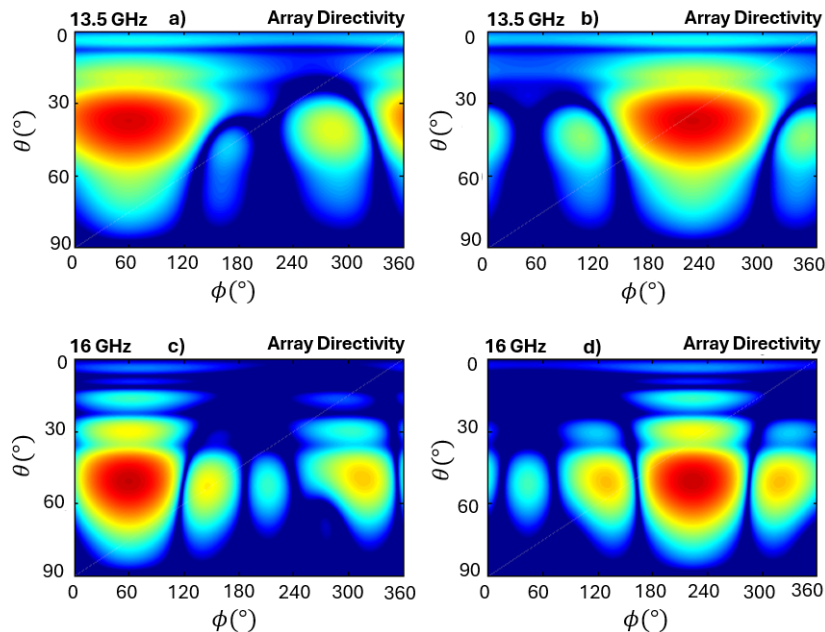


Figure 11. Cont.

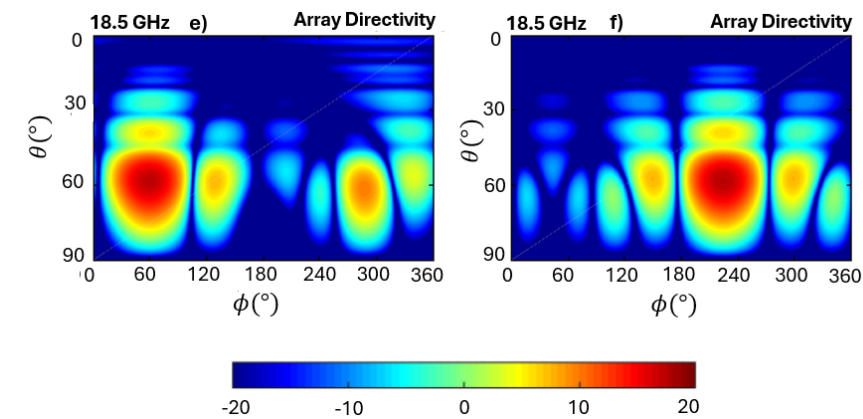


Figure 11. Directivity colormaps in the (ϕ, θ) -plane for an array-fed FPCA, for multiple frequency values and two main beam azimuth planes. (a) $f = 13.5$ GHz, $\phi = 60^\circ$, (b) $f = 13.5$ GHz, $\phi = 225^\circ$, (c) $f = 16$ GHz, $\phi = 60^\circ$, (d) $f = 16$ GHz, $\phi = 225^\circ$, (e) $f = 18.5$ GHz, $\phi = 60^\circ$, (f) $f = 18.5$ GHz, $\phi = 225^\circ$. Reproduced from [46].

When multiple inputs are considered, it is important to assess the cross-coupling among elements. This latter aspect is properly addressed by considering the input scattering matrix, reported in Figure 12 for three independent elements (the others may be deduced by symmetry) [46]. Cross-coupling coefficients have been proven to be lower than -10 dB for adjacent elements, under -18 dB for elements on the same side of the square lattice, and lower than -25 dB for elements at opposite corners. The resulting effect is a bandwidth enhancement, which in turn widens the elevation scan from about 21° to 68° . A full electronic steering effect is achieved with high level of beam directivity using simple and inexpensive materials in compact and easily resizable geometries.

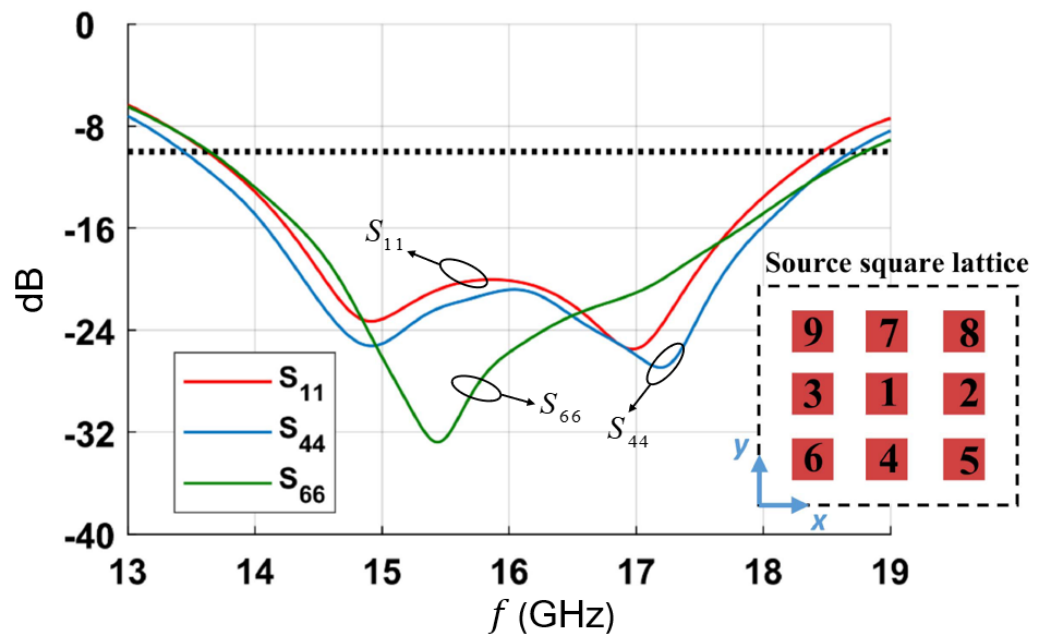


Figure 12. Input reflection coefficients for a 3×3 square planar VEDs array inside an FPCA. The horizontal dashed black line corresponds to the -10 dB threshold. Reproduced from [46].

The fruitful results obtained in [46] turned into a later study presented in [47], with a novel multilayer resonant cavity, where the usual quasi-TEM mode was confined to a slow-wave regime inserting multiple, commercial, low-cost dielectric layers realizing a low-permittivity dielectric constant, as sketched in Figure 13.

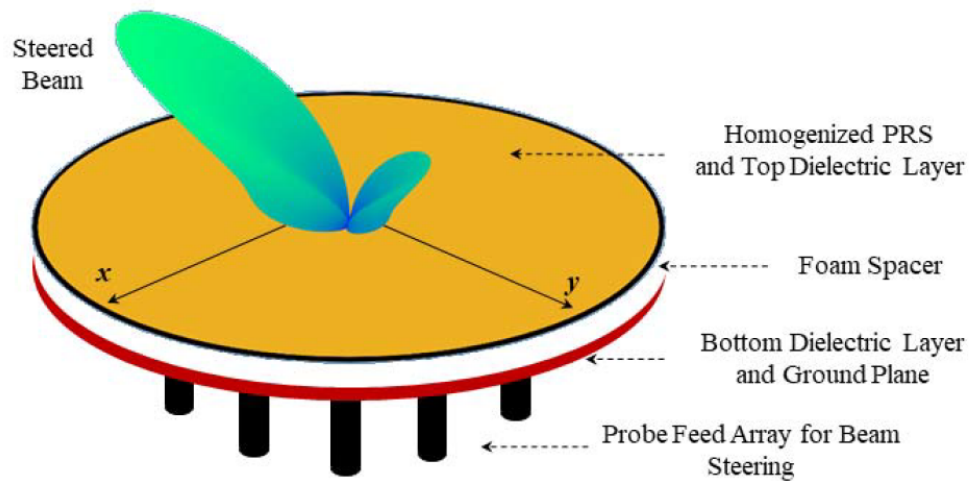


Figure 13. Schematic 2-D sketch of the FPCA structure, with stratified media inside the cavity and homogenized PRS. Multiple coaxial cables are shown as antenna feeders. Reproduced from [47].

Exploiting both the leaky-wave theory and the phased-array theory to separately obtain a scan on elevation and azimuth planes, an increased matching and a shift to higher frequencies of the input reflection coefficient are achieved by concentrically inserting two rings of vias contacting the ground plane of the cavity and the lower dielectric laminate (see Figure 14).

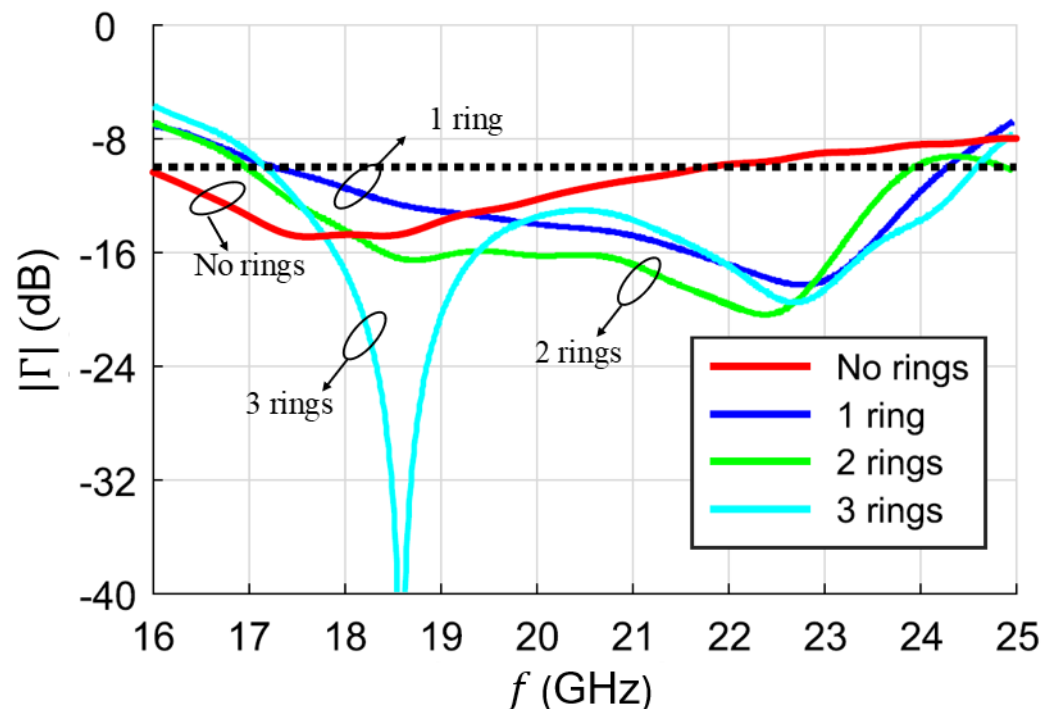


Figure 14. Simulated values for reflection coefficient magnitude, considering different numbers of via-rings. Inserting more concentric rings the reflection coefficient dip shifts to higher frequencies. The horizontal dashed black line corresponds to the -10 dB threshold. Reproduced from [47].

A comparison between square and circular planar arrays was also performed, finding out that the azimuthal symmetry of the latter induces a saturation of the maximum gain obtained by the overall antenna when the number N of coaxial probes is larger than or equal to 6. The circular symmetry of the feeding array impresses full azimuthal stability to the value of the gain; interestingly, the same is true for the first sidelobe level, which remains

stable above a certain number of array elements, maintaining, as the main beam, a perfect symmetry as shown in Figure 15. Additionally, by increasing the number of elements in the source ring, the sidelobe level shows little or no sensitivity after 8 elements are reached. The feeding-network system of a prototype realized with $N = 6$ coaxial cables is shown in Figure 16, where two concentric rings of via holes are inserted to ensure broadband impedance matching.

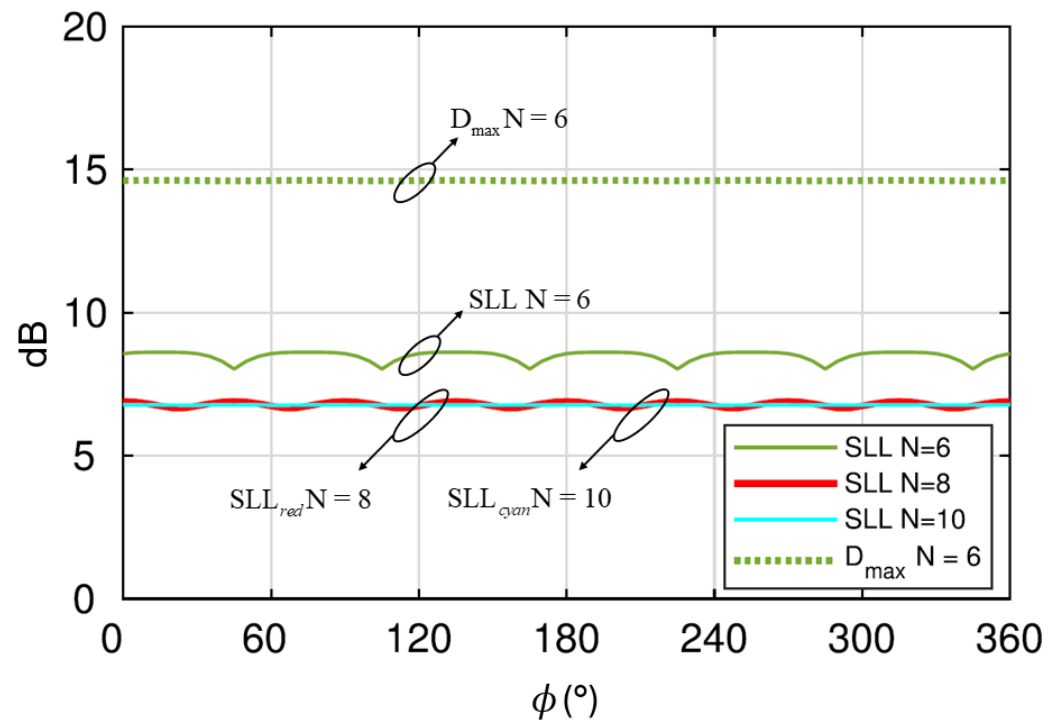


Figure 15. FPCA fed by a circular array with N elements: Simulated maximum directivity for $N = 6$ (green dotted line) and main sidelobe level at 20 GHz for with $N = 6, 8, 10$ (solid lines). Reproduced from [47].



Figure 16. The feeding network realized through a circular array of $N = 6$ coaxial cables. Two concentric via-hole rings are inserted to enhance the broadband impedance matching. Reproduced from [47].

3. Bull's-Eye Antennas

The second class of planar structures considered in this paper consists of *bull's eye* antennas (BEAs).

First proposed in [48], and sketched in Figure 17, BEAs constitute an evolution of the classic grounded dielectric slab, loaded by a certain number (ideally infinite) of concentric,

metallic rings. As a modification of the slab, the typical operative regime consists in exciting the fundamental TM_0 mode which, differently from the case of the simple dielectric slab, may exhibit a radiative fast-wave (i.e., leaky) nature.

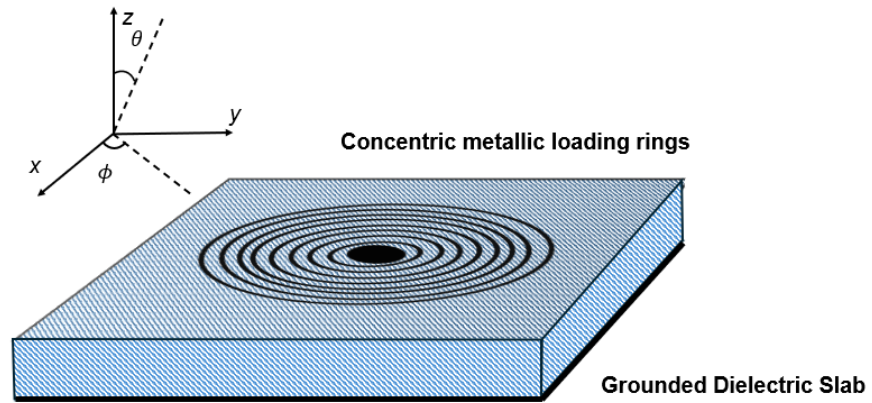


Figure 17. Pictorial representation of a *bull's eye* antenna, constituted by an arrangement of concentric microstrip rings on top of a grounded dielectric slab.

As is known, propagation modes (also known as Bloch modes) in periodic structures are constituted by an infinite number of space harmonics, each one being the solution of the relevant dispersion equation [1]. It is known that, even if the corresponding mode in the unloaded structure is a slow mode, the perturbation due to the periodicity may push, in certain frequency ranges, one or more space harmonics into a fast-wave regime, thus producing radiation leakage. Should one wish to draw a comparison, a BEA is a *radially evolved* classical metal strip grating on a grounded dielectric slab (MSG-GDS) [49–51]. Capable of being excited by simple dipole-like sources as in an FPCA resonant scenario, due to high similarity to the MSG-GDS, the spectral analysis of a BEA may be assumed to be congruent to that performed for the latter. Further details on spectral analysis and design rules can be found in [48].

Among many possible applications, BEAs can be employed in designing near-field focusing devices. As shown in [52,53], a diffraction-limited beam requires an inward cylindrical-wave distribution. Taking advantage of the symmetry properties of Hankel functions recalled by equations in (5), an inward cylindrical-wave distribution can be obtained from an outward cylindrical-wave distribution once a backward leaky wave is excited.

$$H_0^{(2)}(ze^{-j\pi}) = -H_0^{(1)}(z) \quad H_0^{(1)}(ze^{j\pi}) = -H_0^{(1)}(z) \quad (5)$$

Therefore, if a zeroth-order TM cylindrical wave is launched in a BEA through a coaxial feeder, the annular strip grating can be designed to have a space harmonic with a fast and negative phase constant in the desired frequency range. Under such conditions, the BEA is capable of radiating a beam that retains its limited-diffraction properties up to a finite distance known as the nondiffractive range z_{NDR} [54,55].

The microwave and millimeter-wave generation of limited-diffraction beams through BEAs has gained interest for the creation of cutting-edge antenna systems with additional innovative features. For instance, nondiffractive beams, often referred to as Bessel beams (BBs), may carry an OAM, similarly to what happens in the far-field region. While different methods have been proposed to produce such beams, e.g., employing metasurfaces, lenses, and radial line slot arrays [56–59], here we consider array-based solutions. In particular, a novel method to generate OAM-carrying near-field focused beams has been explored considering the insertion of multiple VEDs in the form of a planar, circular coaxial probe array to excite a BEA [60], in order to impress a phase dependence on the azimuth angle of the type $e^{j\ell\phi}$.

Referring specifically to the structure analyzed in [60] and sketched in Figure 18, the dielectric slab is loaded with a number of $N = 13$ metallic rings with a certain width,

which determine a backward-wave regime for the $n = -1$ space harmonic of the perturbed TM_0 mode in a frequency range between 13.5 and 23 GHz. Consequently, by varying the frequency in such a range, a diffraction-robust beam is produced, whose nondiffractive limit is given by $z_{\text{NDR}} = \rho_{\text{BEA}} \cot \theta_0$, with ρ_{BEA} being the radius of aperture and θ_0 corresponding to the so-called axicon angle, approximately determined by the radial leaky phase constant through $\theta_0 = \arcsin(\beta/k_0)$.

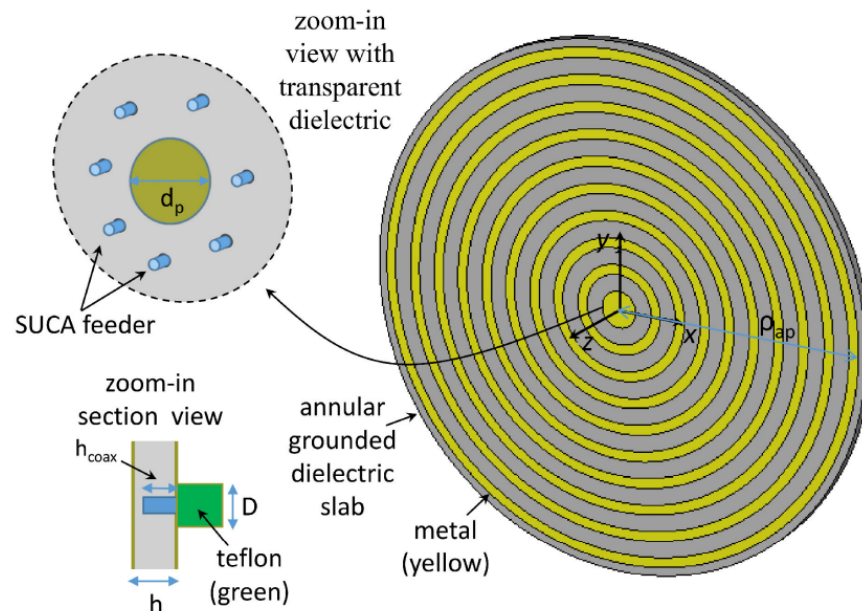


Figure 18. A schematic representation of an array-fed BEA. Coaxial cables in a SUCA configuration provide the excitation to the structure, giving the possibility of OAM reconfiguration. Reproduced from [60].

A systematic issue in problems requiring multiple feeders consists in avoiding cross-coupling among different ports, which is certainly reduced with array thinning. Feeding network design was tackled in [60] and consisted in the single uniform circular array (SUCA) tailoring process, which successfully converged to satisfactory port excitation and OAM purity. Since the BEA does not benefit from translational symmetry, relevant design rules cannot be directly inherited from the case of FPCAs, and a different array radius brings different interactions with metallic rings, thus affecting antenna performance. The optimization process determines a circular array with radius $\rho_{\text{BEA}} = 6$ mm and a number of $N = 8$ VEDs. As displayed in Figure 19, considering the E_θ component, for $|\ell| \leq \pm 3$, the phase constant maintains a linear dependence with respect to ϕ , whereas the amplitude slope remains almost flat, with the only exception being for $\ell = 3$, where some oscillations appear within the ± 3 dB region with respect to the maximum. Finally, magnitude and phase distributions are presented for multiple values of the index ℓ in Figure 20.

The chosen array parameters have proven capable of ensuring a satisfactory feeding, with an average level of -15 dB for the generic scattering parameter S_{ij} and -10 dB for active scattering parameters. This overall design allows us to create a compact device with a satisfactory OAM purity up to z_{NDR} , with OAM order selection possible among $\ell = 0, \pm 1, \pm 2, \pm 3$, with little or no impact on the nondiffractive range for a selected frequency.

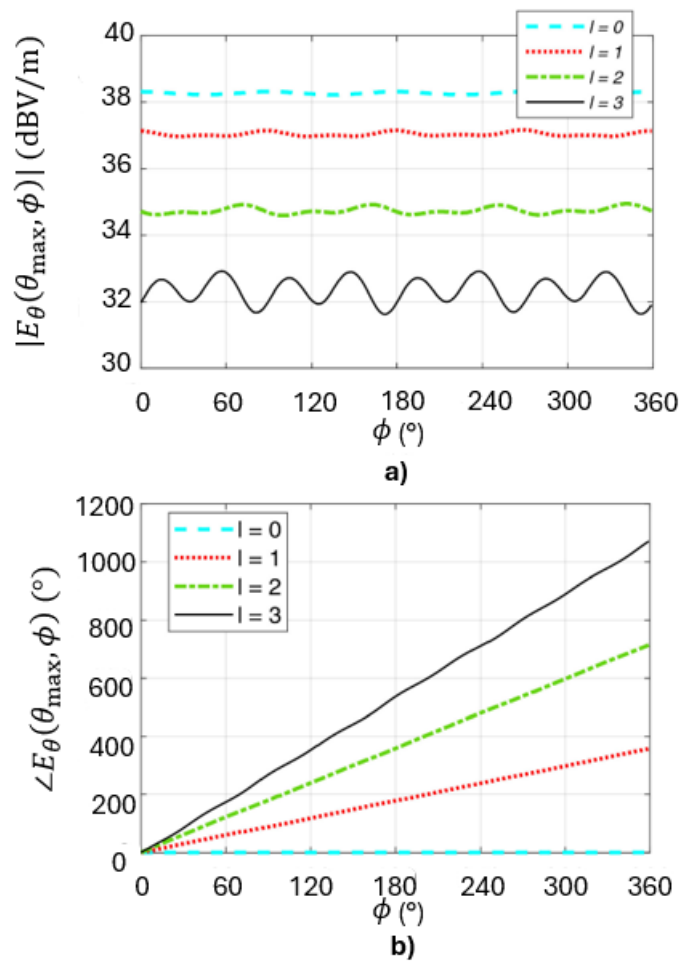


Figure 19. Electric field E_θ along the cone of maximum amplitude $\theta = \theta_{LW}$ radiated by a BEA fed by a circular phased array. (a) Magnitude in dBV/m and (b) phase in degrees. Reproduced from [60].

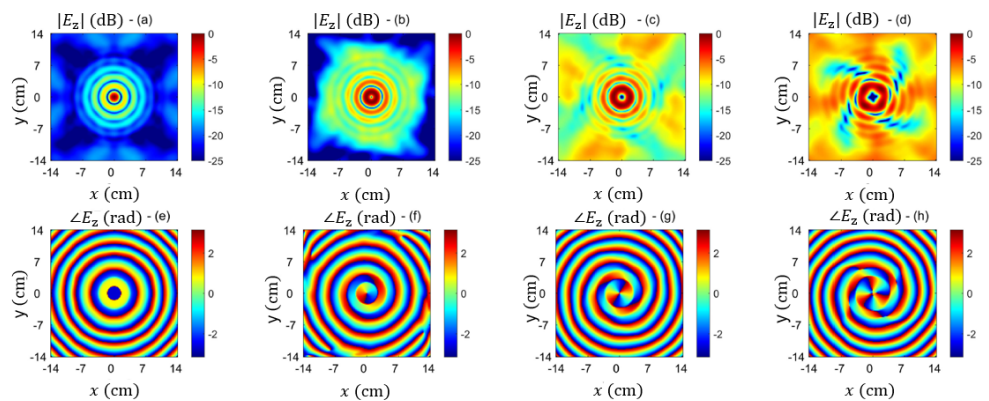


Figure 20. BEA fed by a circular array for the generation of twisted Bessel beams: E_z component magnitude and phase distributions over a transverse $z = z_{NDR}/2$ plane for different azimuthal orders $l = 0, 1, 2, 3$ at a frequency of 18 GHz, with $\beta/k_0 = -0.4$. (a–d) Magnitude (dB). (e–h) Phase (rad). Reproduced from [60].

4. Conclusions

In this paper, several different 2-D planar antenna structures fed by phased arrays have been reviewed, emphasizing the advanced radiative features achieved at limited complexity cost. The common property of the presented devices consists in the excitation of cylindrical leaky waves on the planar surface constituting the antenna aperture. The simplicity in

providing an elevation scan, resulting from the frequency dispersion of relevant supported leaky-mode wavenumbers, greatly simplifies several critical design details, which would otherwise require considerable additional efforts.

The review focused on two categories, Fabry–Perot cavity antennas and *bull’s-eye* antennas, both capable of producing narrow pencil beams at broadside or conical scanned beams.

Array-fed Fabry–Perot cavity antennas have proven capable of achieving reconfigurable far-field polarization, or reconfigurable orbital-angular-momentum order, or 2-D beam scanning in elevation and azimuth.

Bull’s-eye antennas exhibit a richer modal spectrum, allowing for negative radial wavenumbers, corresponding to cylindrical backward leaky waves. This valuable characteristic has been shown to be useful for producing diffraction-resistant Bessel-like beams that, when excited by circular phased arrays, may exhibit a higher azimuthal order and thus carry non-zero orbital angular momentum.

Finally, when compared to traditional phased-array configurations, both considered categories of leaky-wave antennas require a very small number of simple, inexpensive, and broadly available primary radiators, whose reduced complexity substantially simplifies the design and realization of feeding networks.

Author Contributions: Conceptualization, A.G. and P.B.; Methodology, W.F., D.C., A.G. and P.B.; Software, W.F. and D.C.; Formal analysis, P.B.; Investigation, M.M. and E.N.; Data curation, M.M., E.N., W.F. and D.C.; Writing—original draft, M.M.; Writing—review & editing, M.M., E.N., A.G. and P.B.; Visualization, W.F. and D.C.; Supervision, W.F., D.C., A.G. and P.B. All authors have read and agreed to the published version of the manuscript.

Funding: This research was supported by the European Union under the Italian National Recovery and Resilience Plan (NRRP) of NextGenerationEU, partnership on “Telecommunications of the Future” (PE00000001-program “RESTART”).

Data Availability Statement: Data is contained within the article.

Acknowledgments: The authors would like to thank all the co-authors for their valuable contributions and collaboration to the referenced research.

Conflicts of Interest: The authors declare no conflict of interest.

References

- Hessel, A. General characteristics of traveling-wave antennas. In *Antenna Theory, Part 2*; Collin, R.E., Zucker, F.J., Eds.; McGraw-Hill: New York, NY, USA, 1969.
- Jackson, D.R.; Caloz, C.; Itoh, T. Leaky-wave antennas. *Proc. IEEE* **2012**, *100*, 2194–2206. [\[CrossRef\]](#)
- Marcuvitz, N. On field representations in terms of leaky modes or eigenmodes. *IRE Trans. Antennas Propag.* **1956**, *4*, 192–194. [\[CrossRef\]](#)
- Goldstone, L.; Oliner, A.A. Leaky-wave antennas I: Rectangular Waveguides. *IRE Trans. Antennas Propag.* **1959**, *7*, 307–319. [\[CrossRef\]](#)
- Goldstone, L.; Oliner, A.A. Leaky-wave antennas II: Circular Waveguides. *IRE Trans. Antennas Propag.* **1961**, *9*, 280–290. [\[CrossRef\]](#)
- Balanis, C.A. *Advanced Engineering Electromagnetics*; John Wiley & Sons: Hoboken, NJ, USA, 2012.
- Ip, A.; Jackson, D.R. Radiation from cylindrical leaky waves. *IEEE Trans. Antennas Propag.* **1990**, *38*, 482–488. [\[CrossRef\]](#)
- Felsen, L. Real spectra, complex spectra, compact spectra. *JOSA A* **1986**, *3*, 486–496. [\[CrossRef\]](#)
- Fuscaldo, W.; Jackson, D.R.; Galli, A. General formulas for the beam properties of 1-D bidirectional leaky-wave antennas. *IEEE Trans. Antennas Propag.* **2019**, *67*, 3597–3608. [\[CrossRef\]](#)
- Zhao, T.; Jackson, D.R.; Williams, J.T.; Oliner, A.A. General formulas for 2-D leaky-wave antennas. *IEEE Trans. Antennas Propag.* **2005**, *53*, 3525–3533. [\[CrossRef\]](#)
- Tamir, T.; Oliner, A.A. Guided complex waves, Part 1: Fields at an interface. *Proc. Inst. Electr. Eng.* **1963**, *110*, 310. [\[CrossRef\]](#)
- Tamir, T.; Oliner, A.A. Guided complex waves, Part 2: Relation to radiation patterns. *Proc. Inst. Electr. Eng.* **1963**, *110*, 325. [\[CrossRef\]](#)
- Fuscaldo, W.; Burghignoli, P.; Galli, A. Genealogy of Leaky, Surface, and Plasmonic Modes in Partially Open Waveguides. *Phys. Rev. Appl.* **2022**, *17*, 34–38. [\[CrossRef\]](#)
- Fong, B.H.; Colburn, J.S.; Ottusch, J.J.; Visher, J.L.; Sevenpiper, D.F. Scalar and tensor holographic artificial impedance surfaces. *IEEE Trans. Antennas Propag.* **2010**, *58*, 3212–3221. [\[CrossRef\]](#)

15. Martínez-Ros, A.; Gómez-Tornero, J.L.; Goussetis, G. Holographic pattern synthesis with modulated substrate integrated waveguide line-source leaky-wave antennas. *IEEE Trans. Antennas Propag.* **2013**, *61*, 3466–3474. [[CrossRef](#)]
16. Minatti, G.; Caminita, F.; Casaletti, M.; Maci, S. Spiral leaky-wave antennas based on modulated surface impedance. *IEEE Trans. Antennas Propag.* **2011**, *59*, 4436–4444. [[CrossRef](#)]
17. Minatti, G.; Faenzi, M.; Martini, E.; Caminita, F.; De Vita, P.; González-Ovejero, D.; Sabbadini, M.; Maci, S. Modulated metasurface antennas for space: Synthesis, analysis and realizations. *IEEE Trans. Antennas Propag.* **2014**, *63*, 1288–1300. [[CrossRef](#)]
18. Faenzi, M.; Caminita, F.; Martini, E.; De Vita, P.; Minatti, G.; Sabbadini, M.; Maci, S. Realization and measurement of broadside beam modulated metasurface antennas. *IEEE Antennas Wirel. Propag. Lett.* **2015**, *15*, 610–613. [[CrossRef](#)]
19. González-Ovejero, D.; Jung-Kubiak, C.; Alonso-del Pino, M.; Reck, T.; Chattopadhyay, G. Design, fabrication and testing of a modulated metasurface antenna at 300 GHz. In Proceedings of the 11th European Conference on Antennas and Propagation (EUCAP) 2017, Paris, France, 19–24 March 2017; pp. 3416–3418.
20. Fabry, C. Theorie et applications d’une nouvelle methods de spectroscopie interferentielle. *Ann. Chim. Ser. 7* **1899**, *16*, 115–144.
21. Trentini, G.V. Partially reflecting sheet arrays. *IRE Trans. Antennas Propag.* **1956**, *4*, 666–671. [[CrossRef](#)]
22. Jackson, D.R.; Oliner, A.A.; Ip, A. Leaky-wave propagation and radiation for a narrow-beam multiple-layer dielectric structure. *IEEE Trans. Antennas Propag.* **1993**, *41*, 344–348. [[CrossRef](#)]
23. Lovat, G.; Burghignoli, P.; Jackson, D.R. Fundamental properties and optimization of broadside radiation from uniform leaky-wave antennas. *IEEE Trans. Antennas Propag.* **2006**, *54*, 1442–1452. [[CrossRef](#)]
24. James, J.R. Leaky-wave multiple dichroic beamformers. *Electron. Lett.* **1989**, *18*, 1209–1211. [[CrossRef](#)]
25. Feresidis, A.P.; Vardaxoglou, J.C. High gain planar antenna using optimised partially reflective surfaces. *IEE Proc. Microw. Antennas Propag.* **2001**, *148*, 345–350. [[CrossRef](#)]
26. Burghignoli, P.; Fuscaldo, W.; Galli, A. Fabry–Perot Cavity Antennas: The Leaky-Wave Perspective. *IEEE Antennas Propag. Mag.* **2021**, *63*, 116–145. [[CrossRef](#)]
27. Jackson, D.R.; Oliner, A.A. A leaky-wave analysis of the high-gain printed antenna configuration. *IEEE Trans. Antennas Propag.* **1988**, *36*, 905–910. [[CrossRef](#)]
28. Burghignoli, P.; Fuscaldo, W.; Mancini, F.; Comite, D.; Baccarelli, P.; Galli, A. Twisted beams with variable OAM order and consistent beam angle via single uniform circular arrays. *IEEE Access* **2020**, *8*, 163006–163014. [[CrossRef](#)]
29. Su, H.; Shen, X.; Su, G.; Li, L.; Ding, J.; Liu, F.; Zhan, P.; Liu, Y.; Wang, Z. Efficient generation of microwave plasmonic vortices via a single deep-subwavelength meta-particle. *Laser Photon. Rev.* **2018**, *12*, 1800010. [[CrossRef](#)]
30. Yan, Y.; Xie, G.; Lavery, M.P.; Huang, H.; Ahmed, N.; Bao, C.; Ren, Y.; Cao, Y.; Li, L.; Zhao, Z.; et al. High-capacity millimetre-wave communications with orbital angular momentum multiplexing. *Nat. Commun.* **2014**, *5*, 4876. [[CrossRef](#)] [[PubMed](#)]
31. Allen, L.; Beijersbergen, M.W.; Spreeuw, R.; Woerdman, J. Orbital angular momentum of light and the transformation of Laguerre-Gaussian laser modes. *Phys. Rev. Appl.* **1992**, *45*, 8185. [[CrossRef](#)] [[PubMed](#)]
32. Lee, D.; Sasaki, H.; Fukumoto, H.; Yagi, Y.; Shimizu, T. An evaluation of orbital angular momentum multiplexing technology. *Appl. Sci.* **2019**, *9*, 1729. [[CrossRef](#)]
33. Trichili, A.; Park, K.H.; Zghal, M.; Ooi, B.S.; Alouini, M.S. Communicating using spatial mode multiplexing: Potentials, challenges, and perspectives. *IEEE Commun. Surv. Tutor.* **2019**, *21*, 3175–3203. [[CrossRef](#)]
34. Yuan, T.; Wang, H.; Qin, Y.; Cheng, Y. Electromagnetic vortex imaging using uniform concentric circular arrays. *IEEE Antennas Wirel. Propag. Lett.* **2015**, *15*, 1024–1027. [[CrossRef](#)]
35. Burghignoli, P.; Fuscaldo, W.; Comite, D.; Baccarelli, P.; Galli, A. Higher-Order Cylindrical Leaky Waves–Part I: Canonical sources and radiation formulas. *IEEE Trans. Antennas Propag.* **2019**, *67*, 6735–6747. [[CrossRef](#)]
36. Kajiwara, A. Line-of-sight indoor radio communication using circular polarized waves. *IEEE Trans. Veh. Technol.* **1995**, *44*, 487–493. [[CrossRef](#)]
37. Comite, D.; Baccarelli, P.; Burghignoli, P.; Galli, A. Omnidirectional 2-D leaky-wave antennas with reconfigurable polarization. *IEEE Antennas Wirel. Propag. Lett.* **2017**, *16*, 2354–2357. [[CrossRef](#)]
38. Fuscaldo, W.; Galli, A.; Jackson, D.R. Optimization of 1-D unidirectional leaky-wave antennas based on partially reflecting surfaces. *IEEE Trans. Antennas Propag.* **2022**, *70*, 7853–7868. [[CrossRef](#)]
39. Luukkonen, O.; Simovski, C.; Granet, G.; Goussetis, G.; Lioubtchenko, D.; Raisanen, A.V.; Tretyakov, S.A. Simple and accurate analytical model of planar grids and high-impedance surfaces comprising metal strips or patches. *IEEE Trans. Antennas Propag.* **2008**, *56*, 1624–1632. [[CrossRef](#)]
40. Tretyakov, S. *Analytical Modeling in Applied Electromagnetics*; Artech House: Norwood, MA, USA, 2003
41. Mailloux, R.J. *Phased Array Antenna Handbook*; Artech House: Norwood, MA, USA, 2017.
42. Borselli, L.; Di Nallo, C.; Galli, A.; Maci, S. Arrays with widely-spaced high-gain planar elements. In Proceedings of the IEEE Antennas and Propagation Society International Symposium. 1998 Digest. Antennas: Gateways to the Global Network. Held in Conjunction with: USNC/URSI National Radio Science Meeting (Cat. No.98CH36), Atlanta, GA, USA, 21–26 June 1998; Volume 2, pp. 1142–1145.
43. Gardelli, R.; Albani, M.; Capolino, F. Array thinning by using antennas in a Fabry–Perot cavity for gain enhancement. *IEEE Trans. Antennas Propag.* **2006**, *54*, 1979–1990. [[CrossRef](#)]
44. Scattone, F.; Ettore, M.; Fuchs, B.; Sauleau, R.; Fonseca, N.J. Synthesis procedure for thinned leaky-wave-based arrays with reduced number of elements. *IEEE Trans. Antennas Propag.* **2015**, *64*, 582–590. [[CrossRef](#)]

45. Costa, F.; Bianchi, D.; Monorchio, A.; Manara, G. Analytical design of extremely high-gain Fabry-Perot/leaky antennas by using multiple feeds. In Proceedings of the 2017 International Conference on Electromagnetics in Advanced Applications, Verona, Italy, 11–15 September 2017; pp. 1673–1675.
46. Comite, D.; Burghignoli, P.; Baccarelli, P.; Galli, A. 2-D beam scanning with cylindrical-leaky-wave-enhanced phased arrays. *IEEE Trans. Antennas Propag.* **2019**, *67*, 3797–3808. [[CrossRef](#)]
47. Comite, D.; Podilchak, S.K.; Kuznetsov, M.; Buendía, V.G.G.; Burghignoli, P.; Baccarelli, P.; Galli, A. Wideband array-fed Fabry-Perot cavity antenna for 2-D beam steering. *IEEE Trans. Antennas Propag.* **2021**, *69*, 784–794. [[CrossRef](#)]
48. Baccarelli, P.; Burghignoli, P.; Lovat, G.; Paulotto, S. A novel printed leaky-wave ‘Bull’s-Eye’ antenna with suppressed surface-wave excitation. In Proceedings of the IEEE Antennas and Propagation Society Symposium, Monterey, CA, USA, 20–25 June 2004; Volume 1, pp. 1078–1081.
49. Encinar, J.A. Mode-matching and point-matching techniques applied to the analysis of metal-strip-loaded dielectric antennas. *IEEE Trans. Antennas Propag.* **1990**, *38*, 1405–1412. [[CrossRef](#)]
50. Guglielmi, M.; Jackson, D.R. Broadside radiation from periodic leaky-wave antennas. *IEEE Trans. Antennas Propag.* **1993**, *41*, 31–37. [[CrossRef](#)]
51. Burghignoli, P.; Baccarelli, P.; Frezza, F.; Galli, A.; Lampariello, P.; Oliner, A.A. Low-frequency dispersion features of a new complex mode for a periodic strip grating on a grounded dielectric slab. *IEEE Trans. Microw. Theory Tech.* **2002**, *49*, 2197–2205. [[CrossRef](#)]
52. Albani, M.; Pavone, S.C.; Casaletti, M.; Ettore, M. Generation of non-diffractive Bessel beams by inward cylindrical traveling wave aperture distributions. *Opt. Express* **2014**, *22*, 18354–18364. [[CrossRef](#)] [[PubMed](#)]
53. Cai, B.G.; Li, Y.B.; Jiang, W.X.; Cheng, Q.; Cui, T.J. Generation of spatial Bessel beams using holographic metasurface. *Opt. Express* **2015**, *23*, 7593–7601. [[CrossRef](#)] [[PubMed](#)]
54. Ettore, M.; Grbic, A. Generation of propagating Bessel beams using leaky-wave modes. *IEEE Trans. Antennas Propag.* **2012**, *60*, 3605–3613. [[CrossRef](#)]
55. Fuscaldo, W.; Comite, D.; Boesso, A.; Baccarelli, P.; Burghignoli, P.; Galli, A. Focusing Leaky Waves: A Class of Electromagnetic Localized Waves with Complex Spectra. *Phys. Rev. Appl.* **2018**, *9*, 054005. [[CrossRef](#)]
56. Liu, H.; Xue, H.; Liu, Y.; Feng, Q.; Li, L. Generation of high-order Bessel orbital angular momentum vortex beam using a single-layer reflective metasurface. *IEEE Access* **2020**, *8*, 126504–126510. [[CrossRef](#)]
57. Shen, Y.; Yang, J.; Meng, H.; Dou, W.; Hu, S. Generating millimeter-wave Bessel beam with orbital angular momentum using reflective-type metasurface inherently integrated with source. *Appl. Phys. Lett.* **2018**, *112*, 141901. [[CrossRef](#)]
58. Wu, G.B.; Chan, K.F.; Chan, C.H. 3-D printed terahertz lens to generate higher order Bessel beams carrying OAM. *IEEE Trans. Antennas Propag.* **2020**, *69*, 3399–3408. [[CrossRef](#)]
59. Xu, X.; Mazinghi, A.; Freni, A.; Hirokawa, J. Simultaneous generation of three OAM modes by using a RLSA fed by a waveguide circuit for 60 GHz-band radiative near-field region OAM multiplexing. *IEEE Trans. Antennas Propag.* **2020**, *69*, 1249–1259. [[CrossRef](#)]
60. Comite, D.; Fuscaldo, W.; Merola, G.; Burghignoli, P.; Baccarelli, P.; Galli, A. Twisted Bessel beams via bull-eye antennas excited by a single uniform circular array. *IEEE Antennas Wirel. Propag. Lett.* **2021**, *20*, 663–667. [[CrossRef](#)]

Disclaimer/Publisher’s Note: The statements, opinions and data contained in all publications are solely those of the individual author(s) and contributor(s) and not of MDPI and/or the editor(s). MDPI and/or the editor(s) disclaim responsibility for any injury to people or property resulting from any ideas, methods, instructions or products referred to in the content.